Environmental Science and Pollution Research
https://doi.org/10.1007/s11356-021-14880-9

RESEARCH ARTICLE

A new model for settling velocity of non-spherical particles

Fan Yang[1] · Yu-Hong Zeng[1] · Wen-Xin Huai[1]

Received: 23 February 2021 / Accepted: 9 June 2021

Abstract

The settlement of non-spherical particles, such as propagules of plants and natural sediments, is commonly observed in riverine ecosystems. The settling process is influenced by both particle properties (size, density, and shape) and fluid properties (density and viscosity). Therefore, the drag law of non-spherical particles is a function of both particle Reynolds number and particle shape. Herein, a total of 828 settling data are collected from the literatures, which cover a wide range of particle Reynolds number (0.008–10000). To characterize the influence of particle shapes, sphericity is adopted as the general shape factor, which varies from 0.421 to 1.0. By comparing the measured drag with the standard drag curve of spheres, we modify the spherical drag law with three shape-dependent functions to develop a new drag law for non-spherical particles. Combined with an iterative procedure, a new model is thus obtained to predict the settling velocity of non-spherical particles of various shapes and materials. Further applications in hydrochorous propagule dispersal and sediment transport are projected based on deeper understanding of the settling process.

Keywords Drag coefficient · Settling velocity · Sphericity · Non-spherical particles · Particle Reynolds number · Shape-dependent functions

Introduction

In riverine ecosystems, hydrochory plays a major role in transporting and depositing freshly produced plants propagules (predominantly seeds) along the river corridors (Merritt and Wohl 2002; Yoshikawa et al. 2013). In the way of becoming an essential part of the ecosystem, the non-buoyant seeds have to undergo a long period of settling, dispersal, germination, and then gradually contribute to the colonization of the riparian zone (Gurnell et al. 2008; Chambert and James 2009; Koch et al. 2010). Another factor that greatly affects the hydrodynamic process of rivers is the natural sediment. As mentioned by Meier et al. (2013), sediments can promote vegetation growth due to the transportation of nutrients and other organic matters. Moreover, by creating accretional structures in rivers, sediments can also facilitate the development of other species in the new habitats (Gurnell et al. 2012). Thus, as a starting point of the hydrodynamic process, the settlement of both hydrochorous seeds and natural sediments should be paid more attention since the construction of aquatic ecosystem grows more important.

Natural particles are usually generalized as spheres, which simplifies the characterization of particle shapes. Hence, many spherical drag laws, whether explicit or implicit, are proposed by previous studies (Clift and Gauvin 1971; Haider and Levenspiel 1989; Brown and Lawler 2003; Cheng 2009; Terfous et al. 2013). These drag laws reveal that the flow around spherical particles is strongly dependent on the particle Reynolds number. To be more specific, the flow at $Re_p \ll 0.1$ is called the Stokes' regime (or creeping flow), where flow remains attached to the sphere with no wakes behind (White 1998). The flow at $0.1 < Re_p < 1000$ is at the intermediate regime, where the spherical drag coefficient continues to decrease as Re_p increases. At $1000 \le Re_p < 3 \times 10^5$, wakes behind the sphere grow fully turbulent while flow in front of the sphere remains laminar. The flow in this range of Reynolds number is called the Newton's regime (Clift et al. 2005). However, in practical applications, the most commonly encountered particles (e.g., seeds, pebbles, and gravels) are non-spherical and even irregular. Thus, the knowledge of drag

Responsible Editor: Philippe Garrigues

✉ Yu-Hong Zeng
yhzeng@whu.edu.cn

[1] State Key Laboratory of Water Resources and Hydropower Engineering Science, Wuhan University, Wuhan 430072, Hubei, China

Published online: 29 June 2021

coefficient and settling velocity of non-spherical particles is essential for solving the settling problem.

Based on numerous experimental and numerical settling data, many models have been proposed to predict the settling velocities of non-spherical particles. In these models, particles are usually separated into several categories, such as regular-shaped particles (Komar 1980; Haider and Levenspiel 1989; Ganser 1993; Gogus et al. 2001; Wang et al. 2011; Lau and Chuah 2013; Song et al. 2017), natural sediments and crushed rock fragments (Komar and Reimers 1978; Hallermeier 1981; Dietrich 1982; Swamee and Ojha 1991; Chien 1994; Cheng 1997; Alcerreca et al. 2013; Wang et al. 2017), and conglomerates of particles (Tran-Cong et al. 2004). Hence, the performances of most models are restricted in certain types of particles. Moreover, compared to spherical drag coefficients, the drag coefficient of non-spherical particles are determined by parameters other than Re_p, such as particle shape and orientation (Bagheri and Bonadonna 2016). To scale the influence of non-spherical particle shapes, the shape descriptor, aspect ratio (E) is especially designed for the axisymmetric particles, such as cylinders, spheroids, and ellipsoids (Trans-Cong et al. 2004; Loth 2008; Wang et al. 2011). The term S, which is defined as the ratio between equivalent sphere area and the projected area of particle settling direction, is also proposed to describe the effect of settling orientation (Song et al. 2017). However, Bagheri and Bonadonna (2016) found that the impact of both shape and orientation on the non-spherical drag coefficient increases with Re_p, which can be reflected by neither of the two descriptors. They further illustrated that the particle orientation is random in the Stokes' regime, while in the Newton's regime, particle secondary motions and orientation are functions of the particle-to-fluid density ratio, which again proves the insufficiency of the term S. Therefore, it is difficult to generalize the effect of shape and orientation with just one shape descriptor. Another problem for some models is that only part of the flow regimes is covered due to the limitation of experimental conditions. For instance, the model of Wang et al. (2017) is applicable for particle Reynolds numbers in the range of 0.01 to 3700, which covers Stokes', intermediate, and early stage of Newton's flow regime. As for particles that settle in higher stage of Newton's regime, the prediction ability of the model is unknown.

To solve the above-mentioned problems, a reliable model is developed based on a large amount of settling data, including mineral sediments and artificial particles. Note that behaviors of non-buoyant seeds during entrainment and settling are consistent with that of mineral sediments, and the settling process of such artificial particles is analogous to that of natural sediments (Zhu et al. 2017). Herein, the shape descriptor, sphericity, is used as the general parameter to show the influence of particle shapes. Note that the sphericity of these particles varies from 0.421 to 1.0. In addition, the particle Reynolds number ranges from 0.008 to 10000, which almost covers all regimes that can be encountered in natural processes. Herein, we modify the spherical drag law of Clift and Gauvin (1971) with shape-related functions to produce a new drag law for non-spherical particles. Subsequently, with an iterative procedure, a new model is developed to predict the settling velocity for different types of particles, which can eventually be applied in understanding the deposition, transport, and dispersal of seeds and natural sediments.

In situ settling velocity

For particles settling through a static fluid, the balance between surface (drag) and body forces acting on the particle is expressed as follows:

$$\frac{1}{2}\rho_f C_d A_p W_s^2 = \left(\rho_s - \rho_f\right) gV \tag{1}$$

Therefore, the settling velocity of the particle can be obtained through the following formula:

$$W_s = \sqrt{\frac{4\left(\rho_s - \rho_f\right) g d_n}{3\rho_f C_d}} \tag{2}$$

where ρ_f is the fluid density, ρ_s is the particle density, C_d is the drag coefficient depending on properties of particle and fluid, A_p is the projected area of the particle perpendicular to the settling direction, W_s is the settling velocity of the particle, g is the gravitational acceleration, and V is the volume of the particle.

The particle Reynolds number (R_{ep}) is defined as:

$$R_{ep} = \frac{\rho_f W_s d_n}{\mu} \tag{3}$$

where d_n is the diameter of the volume equivalent sphere, and μ is the dynamic viscosity of the fluid.

Particle shape characterization

The nominal diameter of non-spherical particles (d_n) can be calculated as the diameter of the sphere whose volume is equivalent to the non-spherical particle's volume (Wadell 1932).

$$d_n = \sqrt[3]{6V/\pi} \tag{4}$$

To describe the shape of non-spherical particles, multiple shape descriptors are proposed, which can be divided in 1D, 2D, and 3D shape descriptors. 1D descriptors are called form factors, which are based on particle lengths in three dimensions (i.e., d_s, d_m, d_l, which are the short, medium, and long principle axes of the particle, respectively). Form factors

include flatness ($f = d_s/d_m$) and elongation ($e = d_m/d_l$) (Loth 2008; Bagheri et al. 2015). The Corey shape factor ($CSF = d_s/\sqrt{d_l d_m}$) is the most commonly used 1D descriptor that describes particles of relatively smooth surfaces (Corey 1963; Swamee and Ojha 1991). As a 2D descriptor, circularity (X) is based on 2D variables obtained by image analysis, which is suitable for particles with sharp corners and large obtuse angles (Büttner et al. 2002). Circularity is defined as the ratio between the maximum projection perimeter P_{mp} and that of the perimeter of the circle equivalent to the maximum projection area P_{eq}:

$$X = \frac{P_{mp}}{P_{eq}} \tag{5}$$

where P_{mp} and P_{eq} are calculated by approximating the maximum projective regions as ellipses, with the former determined by $\pi\sqrt{d_l d_m}$. The latter P_{eq} can be calculated by the first approximation by Ramanujan (1914), which is expressed as:

$$P_{mp} \approx \pi \left[3(d_l + d_m) - \sqrt{10 d_l d_m + 3\left(d_l^2 + d_m^2\right)}\right] \tag{6}$$

Sphericity (ϕ), which is related to the surface area and particle volume, is considered as a 3D shape descriptor. Applied in settling models where particles are of various shapes and materials, sphericity is proved to be the best parameter to describe the influence of particle shape, and thus is chosen in this study (Haider and Levenspiel 1989; Ganser 1993; Chien 1994). Sphericity is defined as the ratio between the surface area of the equivalent sphere A_{sph} and the particle surface area A_s:

$$\phi = \frac{A_{sph}}{A_s} \tag{7}$$

where A_{sph} is calculated by $A_{sph} = 4\pi(d_n/2)^2$.

For particles that are similar to scalene ellipsoids, the surface area of particle A_s can be approximately calculated as follows (Taylor et al. 2006):

$$A_s \approx 4\pi \left[\frac{(ab)^\lambda + (ac)^\lambda + (bc)^\lambda}{3 - k\left(1 - 27abc(a+b+c)^{-3}\right)}\right]^{1/\lambda} \tag{8}$$

where a, b, and c are semi-axes of a tri-axial ellipsoid, λ=1.5349, k=0.0942.

Except for ϕ, another frequently used 3D shape descriptor is ψ, which is defined as the ratio between sphericity and circularity ($\psi = \phi/X$). This descriptor is first introduced by Dellino et al. (2005) for highly irregular particles, and its validity has been verified by Dioguardi and Mele (2015) and Dioguardi et al. (2018).

Materials and methods

Formulation

To develop a new shape-dependent drag law, we collect 828 sets of settling data from previous studies (Komar and Reimers 1978; Komar 1980; Baba and Komar 1981; Chambert and James 2009; Koch et al. 2010; Wang et al. 2011; Dioguardi and Mele 2015; Song et al. 2017; Zhu et al. 2017). Details of the dataset are listed in Table 1. Note that within the database, the range of ϕ is 0.421–1.0, and the value of R_{ep} varies from 0.008 to 10000.

Settling data of regular particles, such as cylinders, cuboids, cubes, and disks, are collected from Komar (1980), Wang et al. (2017), and Song et al. (2017). In these cases, the geometric parameters of particles are provided, which means both circularity and sphericity can be calculated through the definitions of P_{mp}, P_{eq}, A_{sph}, and A_s. In contrast, data from Komar and Reimers (1978) and Baba and Komar (1981) are aimed at irregular-shaped particles, such as pebbles and glasses. Herein, weight and tri-axial lengths of the particle (d_s, d_m, d_l) are given, as well as particle density (ρ_s). Thus, the corresponding circularity and sphericity can be obtained using the approximated equations (Eq. (5)~Eq. (8)). As for volcanic particles in Dioguardi and Mele (2015), three shape descriptors (X, ϕ, ψ) are provided directly, as well as d_s, d_m, d_l. In light of the hydrochorous seeds in Chambert and James (2009), Koch et al. (2010), and Zhu et al. (2017), the values of sphericity are listed directly, along with the volume equivalent spherical diameter (d_n). Thus, in the case of seeds, both X and ψ cannot be obtained without more information of d_s, d_m, d_l.

Enlightened by the idea of Dioguardi et al. (2018), we construct a new drag law for non-spherical particles based on the spherical drag law of Clift and Gauvin (1971). This spherical drag law is chosen since it can effectively cover the entire R_{ep} range of the standard drag curve.

$$C_{d,sphere} = \frac{24}{R_{ep}}\left(1 + 0.15R_{ep}^{0.687}\right) + \frac{0.42}{1 + \frac{42500}{R_{ep}^{1.16}}} \tag{9}$$

By comparing the difference between the measured drag coefficient ($C_{d,\ meas}$) in our database and the drag of a sphere ($C_{d,\ sphere}$) at the same R_{ep}, we separate Eq. (7) into the sum of three terms:

$$C_{d,sphere} = \frac{24}{R_{ep}} + \frac{24}{R_{ep}}\left(0.15R_{ep}^{0.687}\right) + \frac{0.42}{1 + \frac{42500}{R_{ep}^{1.16}}} \tag{10}$$

In Fig. 1, we plot the measured drag coefficient of particles $C_{d,\ meas}$ versus the drag curve for spheres. The drag of non-spherical particles is observed to be larger than $C_{d,\ sphere}$ in

Table 1 Sources of data

Source	Number of points	Particle types
Song et al. (2017)	276	Cube, cylinder, disk
Dioguardi and Mele (2015)	340	Volcanic materials
Wang et al. (2011)	48	Cuboids
Komar and Reimers (1978)	51	Ellipsoidal pebbles
Baba and Komar (1981)	72	Irregular glass particles
Komar (1980)	27	Cylindrical-shaped grains
Chambert and James (2009)	8	Non-spherical seeds
Koch et al. (2010)	3	Non-spherical seeds
Zhu et al. (2017)	3	Non-spherical seeds

most cases. Specifically, the measured drag (black dots) is close to $C_{d,\ sphere}$ (solid line) for R_{ep}<10. As R_{ep} grows larger than 10, the bias between the measured drag and the standard drag curve also becomes larger, since the influence of particle orientation and irregularity on the non-spherical drag coefficient increases with R_{ep} (Bagheri and Bonadonna 2016). In addition, for irregular particles whose sphericities are near 1.0, their corresponding black dots on the figure are also closely related to the standard spherical drag curve. From these observations, we hypothesize that the influence of particle shape can be separately added to the three parts of Eq. (10), as has been done by Dioguardi et al. (2018). Note that the shape descriptors (ϕ) in these functions are different from that (ψ) in the functions of Dioguardi et al. (2018).

$$C_{d,calc} = \frac{24}{R_{ep}} f_1(\phi) + \frac{24}{R_{ep}}\left(1 + 0.15{R_{ep}}^{0.687}\right) f_2(\phi) + \frac{0.42}{1 + \frac{42500}{{R_{ep}}^{1.16}}} f_3(\phi) \quad (11)$$

For the shape-modified functions, the following constraints must be satisfied.

$$f_1(\phi = 1) = f_2(\phi = 1) = f_3(\phi = 1) = 1 \quad (12)$$

Therefore, when the shape of a particle is close to a sphere ($\phi \approx 1$), Eq. (11) can turn back to the spherical drag law (Eq.

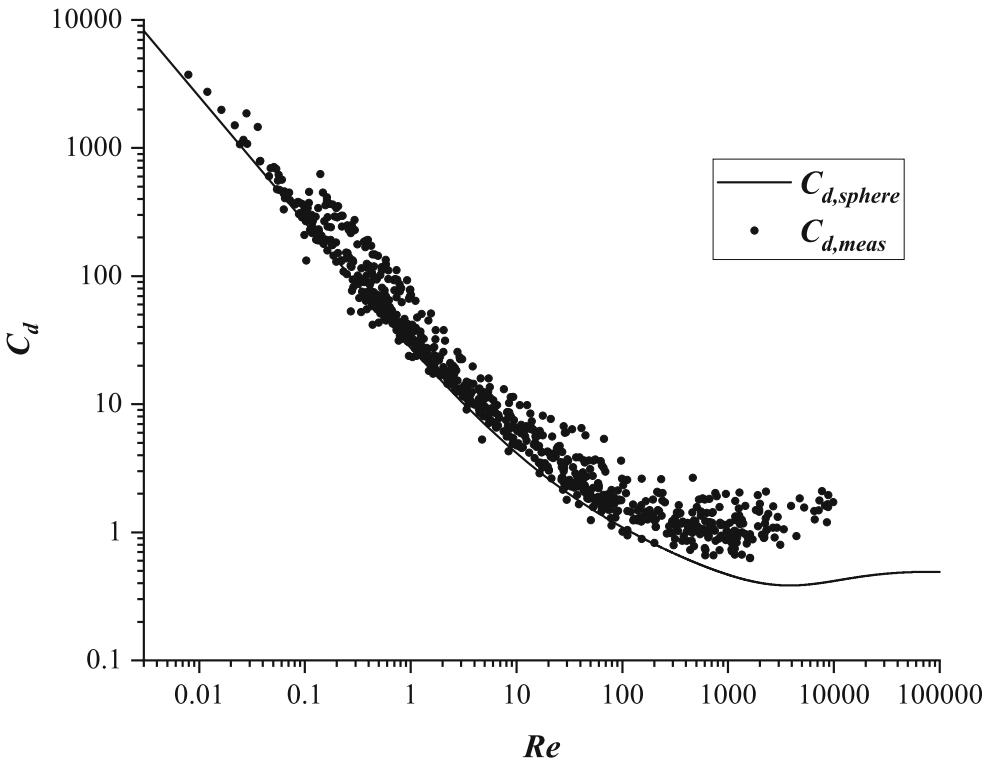

Fig. 1 C_d versus R_e log-log plot showing the measured drag coefficient of particles in our database $C_{d,meas}$ (black dots) and the standard drag curve for a sphere as defined by Clift and Gauvin (1971) (solid line)

(10)). Based on the collected database, the three functions are obtained by comparing the difference between $C_{d,\ meas}$ and $C_{d,\ sphere}$ focusing on the three parts separately. Following the assumption of Dioguardi et al. (2018), we also assume that the ratio between each terms of $C_{d,\ sphere}$ and the total $C_{d,\ sphere}$ is equal to the ratio between each part of $C_{d,\ meas}$ and the total drag of non-spherical particles (see Eq. (13)).

$$\frac{C_{d,sphere}(part)}{C_{d,sphere}(total)} = \frac{C_{d,meas}(part)}{C_{d,meas}(total)} \tag{13}$$

With this assumption, the three functions are separately searched by correlating each part of $C_{d,\ calc}$ with ϕ and R_{ep}. The best function is the one with the minimum error when predicting the settling velocity $W_{s,\ meas}$. Finally, the three functions satisfying the constraints and assumptions are:

$$f_1(\phi) = (2-\phi)^{\alpha_1} \tag{14a}$$

$$f_2(\phi) = \phi^{-R_{ep}{}^{\alpha_2}} \tag{14b}$$

$$f_3(\phi) = e^{\alpha_3(1-\phi)} \tag{14c}$$

The values of three exponents a_1, a_2, and a_3 are obtained by iteratively searching for the values that can present the best fit with the measured data. The iterative searching process is conducted with the Matlab script. The best values of a_1, a_2, and a_3 are 1.29, 0.134, and 1.43, respectively.

Thus, Eq. (11) turns to the new drag law:

$$C_{d,calc} = \frac{24}{R_{ep}}(2-\phi)^{1.29} + \frac{24}{R_{ep}}\left(1+0.15{R_{ep}}^{0.687}\right)\phi^{-{R_{ep}}^{0.134}} + \frac{0.42}{1+\frac{42500}{{R_{ep}}^{1.16}}}e^{1.43(1-\phi)} \tag{15}$$

As an implicit drag law depending on R_{ep}, an iterative procedure is usually adopted for calculating C_d, since both C_d and R_{ep} are relevant to W_s. The trial-and-error procedure is presented in the flow chart (Fig. 2). Details of the new drag law can be found in the Online Resource (sheet of "Drag law").

Models for comparison

To evaluate the ability of the present model to predict the settling velocity of non-spherical particles, we compare it with previous models (Chien 1994; Alcerreca et al. 2013; Dioguardi and Mele 2015; Dioguardi et al. 2018). Details of comparison with other models are given in the Online Resource (sheet of "Model comparison").

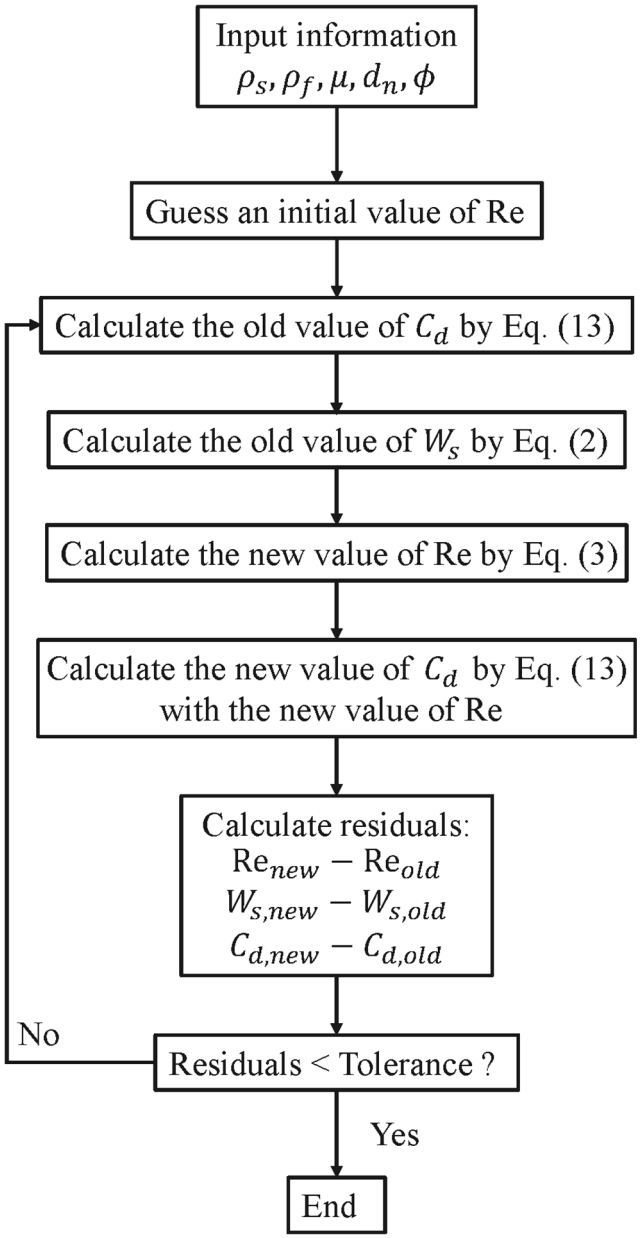

Fig. 2 Flow chart of the trial-and-error procedure for the calculation of C_d

Chien (1994) derived the drag law for irregular particles settling in Newtonian and non-Newtonian fluids. Since this drag law is also implicit, a numerical iteration method is required to predict the settling velocity. The model of Chien (1994) covers a ϕ range of 0.2–1.0, and a R_{ep} range of 0.001–10000.

$$C_d = \frac{30}{R_{ep}} + \frac{67.289}{e^{5.03\phi}} \tag{16}$$

The drag law of Alcerreca et al. (2013) is derived based on a large amount of settling data of calcareous sand particles. The drag law is explicit since C_d can be expressed as a function of the dimensionless particle diameter D_*:

$$C_d = \frac{4}{3}\frac{D_*^3}{{R_{ep}}^2} \tag{17a}$$

$$R_{ep} = \frac{\rho_f W_s d_n}{\mu} = \left(\sqrt{22 + 1.13D_*^2} - 4.67\right)^{1.5} \tag{17b}$$

$$D_* = d_N\left[\left(g/\upsilon^2\right)\left(\rho_s/\rho_f - 1\right)\right]^{1/3} \tag{17c}$$

where d_N is the nominal particle diameter which can be calculated by $d_N = (d_l d_m d_s)^{1/3}$, and υ is the kinematic viscosity of the fluid. Consequently, the settling velocity can be calculated directly from basic properties of particles and fluids (d_l, d_m, d_s, ρ_s, ρ_f, υ).

According to the detailed dataset description in the "Formulation" section, the law of Alcerreca et al. (2013) can be applied directly in volcanic materials, pebbles, and glass particles, the basic properties of which have all been provided. For regular particles involved in the dataset, their form dimensions (d_l, d_m, d_s) are shown in Table 2, which enable the application of Alcerreca et al. (2013). As for hydrochorous seeds, d_N can be directly replaced by the volume equivalent spherical diameter d_n.Thus, the drag law of Alcerreca et al. (2013) can be applied in the whole dataset.

Dioguardi and Mele (2015) applied the shape descriptor ψ to describe the irregularity of particles. Their drag law is based on the 340 settling data of volcanic particles, which are in a wide range of D_* (0.03–10000). Developed from the drag law of Dellino et al. (2005), the form of this law is segmented and simple:

$$C_d = \frac{C_{d,sphere}}{{R_{ep}}^2 \psi^{\exp}}\left(\frac{R_{ep}}{1.1883}\right)^{\frac{1}{0.4826}} \tag{18}$$

$\exp = {R_{ep}}^{-0.23}$ for the R_{ep} ranges of 0–50;

$\exp = {R_{ep}}^{0.05}$ for the R_{ep} ranges of 50–10000;where $C_{d,sphere}$ is calculated by the drag law of Clift and Gauvin (1971) (see Eq. (9)). An iterative procedure is needed to construct the final model to predict the terminal settling velocity.

As a development of Dioguardi and Mele (2015), the model of Dioguardi et al. (2018) also used the shape descriptor ψ. Their drag law is obtained by 304 settling velocity measurements, which are part of the 340 settling data mentioned in Table 1. Note that the structure of this model is similar to the present model (Eq. (15)). Differences between the two models are discussed in the "Discussion" section.

$$C_{d,calc} = \frac{24}{R_{ep}}\left(\frac{1-\psi}{R_{ep}} + 1\right)^{0.25} + \frac{24}{R_{ep}}\left(0.1806{R_{ep}}^{0.6459}\right)\psi^{-\left({R_{ep}}^{0.08}\right)} + \frac{0.4251}{1 + \frac{6880.95}{R_{ep}}\psi^{5.05}} \tag{19}$$

Comparison results

To compare the accuracy of predicting the settling velocity for each model, we first plot the $C_{d,\ calc}$ and $C_{d,\ meas}$ versus R_{ep} in Fig. 3. After calculating the $C_{d,\ calc}$ with the aforementioned laws, we iteratively obtain the terminal settling velocity $W_{s,\ calc}$ and compare it with the measured values $W_{s,\ meas}$. In Fig. 4, the comparison results are displayed, along with the correlation coefficient of each model. As shown in Fig. 4, most models have similar correlation coefficients, which are approximately 0.94. The performance of Alcerecca et al. (2013) is relatively weak, which may due to the fact that their model is based on settling data of calcareous sand. Thus, for non-spherical particles of other shapes and materials, the ability of this model to predict the settling velocity is limited. Both Fig. 3 and Fig. 4 are presented following the idea of Dioguardi et al. (2018).

Based on the correlations between $W_{s,\ calc}$ and $W_{s,\ meas}$, three statistical parameters are used as indicators to assess the ability of different models to predict the settling velocity of non-spherical particles. The first parameter is the R-squared (R^2), which is obtained by linear fitting and presented in Fig. 4 for each model. The second parameter is average absolute error (|err%|), which is calculated as follows:

$$|err\%| = \frac{\left|W_{s,calc} - W_{s,meas}\right|}{W_{s,meas}} \times 100 \tag{20}$$

Table 2 Nominal diameter and form dimensions of some geometrical shapes involved in the dataset. The edge lengths of cubes and cuboids are s and h ($s \le h$, $s = h$ in the case of cubes). The diameter and height of cylinders and disks are d and l ($d < l$ for cylinders, $d > l$ for disks), respectively

Shape	d_n	d_l	d_m	d_s
Cube	~1.24s	$\sqrt{2}s$	$\sqrt{2}s$	s
Cuboid	$\sqrt[3]{6s^2h/\pi}$	$\sqrt{s^2+h^2}$	$2sh/\sqrt{s^2+h^2}$	s
Cylinder	$\sqrt[3]{3d^2l/2}$	$\sqrt{d^2+l^2}$	l	d
Disks	$\sqrt[3]{3d^2l/2}$	$\sqrt{d^2+l^2}$	d	l

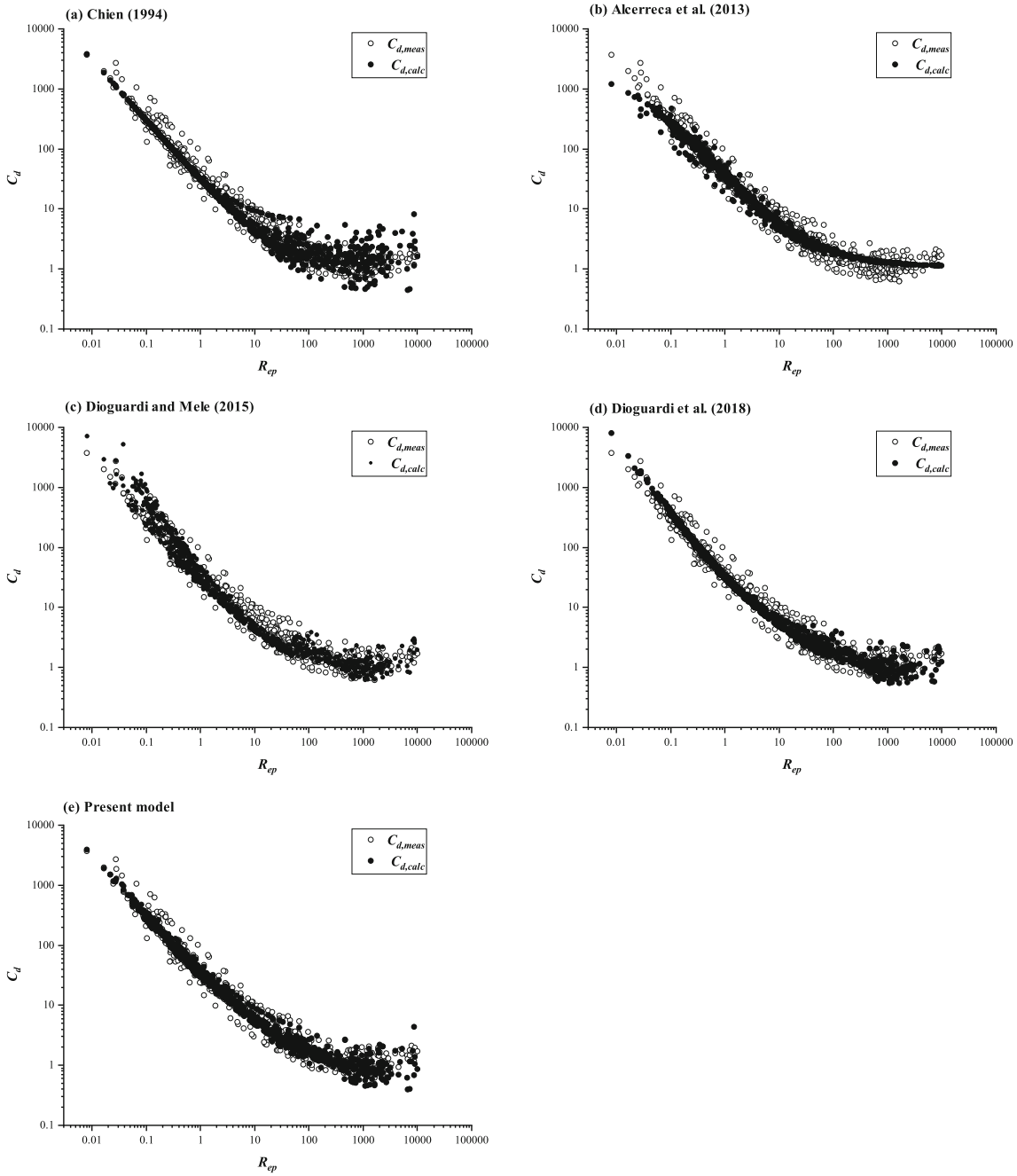

Fig. 3 **a**–**e** Plot of C_d versus R_{ep} for previous and present models. The empty circles represent $C_{d,meas}$ and the solid circles represent $C_{d,calc}$

We also evaluate each model with the root-mean-square error (RMSE) by applying the following formula:

$$RMSE = \sqrt{\frac{\sum_{i=1}^{N}\left(\frac{W_{s,calc,i}-W_{s,meas,i}}{W_{s,meas,i}}\right)^2}{N}} \times 100 \quad (21)$$

where N=828 is the number of settling data in our database.

Error analyses of the three indicators for different models are summarized in Table 3. From R^2 listed in Table 3, the performance of the present model is slightly weaker than the model of Dioguardi et al. (2018). However, when evaluating the performance of models by |err%| and RMSE, the present model predicts the settling velocity better than all the other models.

To further explore the differences among these models, we compare the ability of each model to predict settling velocity of particles from different sources. The comparisons of |err%| are given in Table 4 while the results of RMSE are summarized in Table 5. About the two tables, two notations are

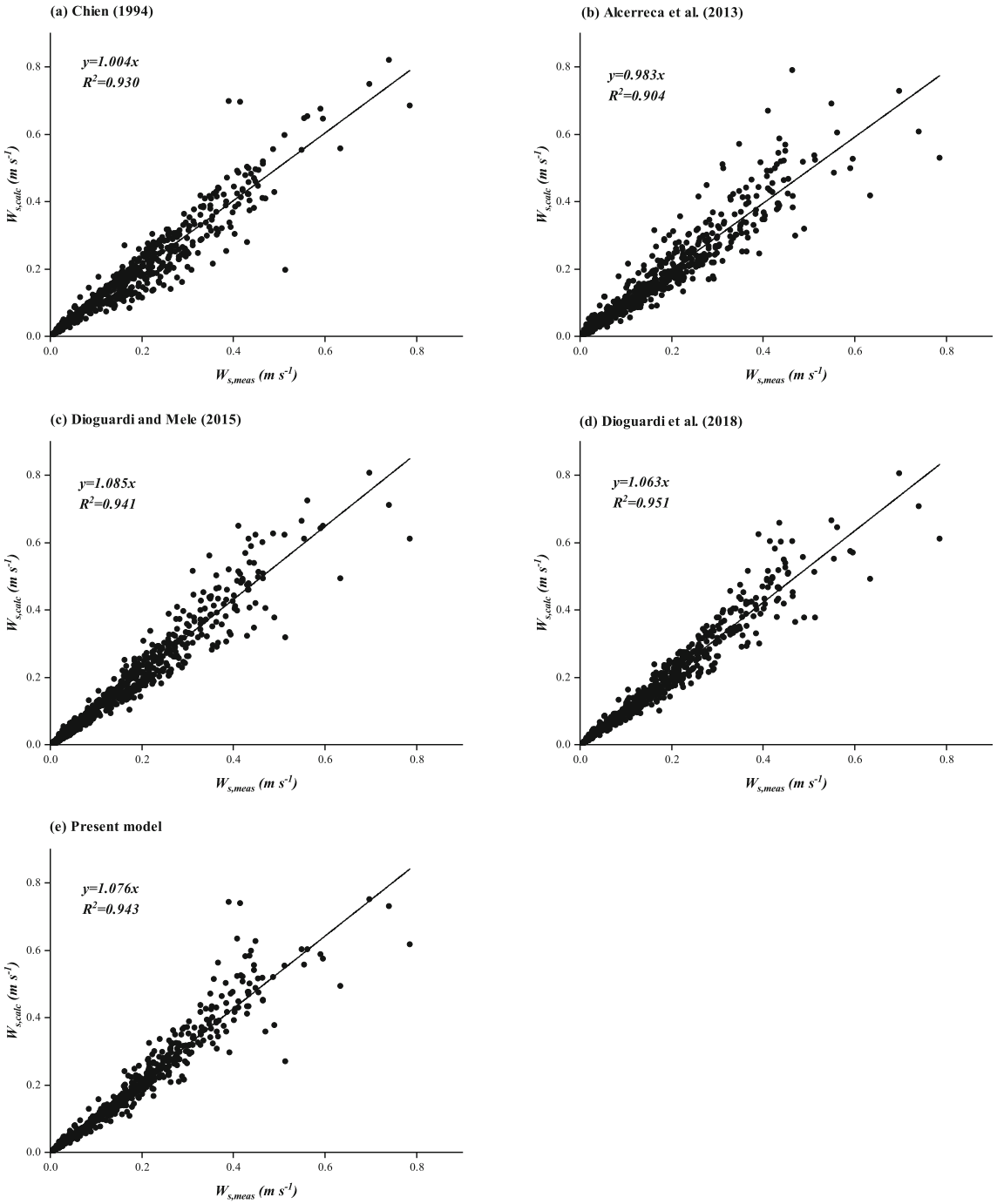

Fig. 4 **a**–**e** Plot of $W_{s,calc}$ versus $W_{s,meas}$ for previous and present models. The solid line is the best fit line of type $y=ax$. The line relations are also reported with R^2

clarified. Firstly, since the number of settling data of hydrochorous seeds is low, we summarize the settling data of seeds from three sources in one row, which is simply marked as "hydrochorous seeds" (Chambert and James 2009; Koch et al. 2010; Zhu et al. 2017). Secondly, since the data of tri-axial lengths are missing for hydrochorous seeds, the shape descriptor ψ mentioned in the models of Dioguardi and Mele (2015) and Dioguardi et al. (2018) cannot be calculated without approximated values of circularity. Thus, in the last row of both tables, the error analyses for hydrochorous seeds are not given for the two models.

From Tables 4 and 5, the present model performs quite well for data collected from Song et al. (2017), Komar and Reimers (1978), and Baba and Komar (1981). Combined with particle shapes and materials listed in Table 1, the present model is found to be especially suitable for regular particles (e.g., cubes and

Table 3 Performance comparison of models

Model	R^2	|err%|	RMSE
Chien (1994)	0.930	13.347	18.664
Alcerreca et al. (2013)	0.904	18.270	28.098
Dioguardi and Mele (2015)	0.941*	16.186*	20.142*
Dioguardi et al. (2018)	0.951*	11.652*	15.800*
Present model	0.943	9.624	15.061

Note: Data marked with asterisk are obtained without considering the settlement of hydrochorous seeds. The data are still convincible since the settling data of seeds (14 data points) only account for 1.69% of the total database (828 data points)

cylinders) and particles with relatively smooth surfaces (e.g., pebbles and irregular glass particles). Nevertheless, the accuracy of the present model to predict the settling velocities for data from Wang et al. (2011), Komar (1980), and hydrochorous seeds is only acceptable. For data from Wang et al. (2011) and Komar (1980), the present model performs better than the other models except for the model of Dioguardi and Mele (2015). The prediction for settling velocity of hydrochorous seeds, though not accurate enough, is the best among these models. A common reason for the deviations is that all the settling data from the three sources are no more than 50 data points, and thus the errors may be enlarged. At last, the abilities of the models to predict settling velocity of volcanic particles are compared. Since the models of both Dioguardi and Mele (2015) and Dioguardi et al. (2018) are developed from the settling data of volcanic materials, they naturally show smaller errors than the other models. Note that the performance of the present model is just slightly weaker than the two models. To summarize from the above analysis, it can be concluded that the present model shows the best performance when predicting settling velocity for particles of various shapes and materials.

Discussion

Among these models for comparison, the differences between the model of Dioguardi et al. (2018) and the present model need to be further discussed, since they are based on similar ideas. Herein, four major differences are clarified. Firstly, as shown in Table 1, the present model contains a larger database, which includes particles of various shapes and materials. On the other hand, the model of Dioguardi et al. (2018) is based on only part of the 340 data points of volcanic particles. Secondly, the shape descriptor applied by Dioguardi et al. (2018) is ψ rather than ϕ. As mentioned in the "Particle shape characterization" section, the calculation of ψ requires the value of circularity (X) in addition to sphericity (ϕ). Thus, the model of Dioguardi et al. (2018) has more difficulty in application. Thirdly, the first and last shape-modified functions of the present model ($f_1(\phi)$ and $f_3(\phi)$ in Eq. (15)) have different forms and positions with that of the model of Dioguardi et al. (2018) (Eq. (19)). Lastly, the model of Dioguardi et al. (2018) is based on the spherical drag law of Haider and Levenspiel (1989), which is suitable for $R_{ep} < 2.6 \times 10^5$.

Developed from the idea of Dioguardi et al. (2018), the present model enhances the applicability in predicting the terminal settling velocity for particles of various shapes and materials, and thus can be considered as an improvement.

Conclusion

We propose a new drag law for non-spherical particles based on a total of 828 settling data collected from previous studies (Komar and Reimers 1978; Komar 1980; Baba and Komar 1981; Chambert and James 2009; Koch et al. 2010; Wang et al. 2011; Dioguardi and Mele 2015; Song et al. 2017; Zhu et al. 2017). This new database cover a R_{ep} range of 0.008~10000 and a ϕ range of 0.421~1.0. Thus, the new model is suitable for the settlement of non-spherical particles in both laminar and turbulent flows. In addition, since this new model is developed from settling data from various sources, it can be applied in predicting settling velocity of regular particles (e.g., cubes, cylinders, disks, and cuboids), natural particles (e.g., volcanic particles, pebbles, and glass particles of various shapes), and even non-spherical hydrochorous seeds.

Table 4 Comparisons of models by |err%|

Data source	Chien (1994)	Alcerecca et al. (2013)	Dioguardi and Mele (2015)	Dioguardi et al. (2018)	Present model
Song et al. (2017)	22.790	13.507	17.314	12.23	7.234
Dioguardi and Mele (2015)	15.233	14.701	11.123	10.69	11.587
Wang et al. (2011)	16.747	15.646	20.800	16.25	17.627
Komar and Reimers (1978)	8.407	4.847	24.692	7.35	2.590
Baba and Komar (1981)	9.733	3.418	25.356	10.30	3.790
Komar (1980)	54.307	27.107	19.701	21.394	20.435
Hydrochorous seeds	18.455	24.914	/	/	16.424

Table 5 Comparisons of models by RMSE

Data source	Chien (1994)	Alcerecca et al. (2013)	Dioguardi and Mele (2015)	Dioguardi et al. (2018)	Present model
Song et al. (2017)	36.102	18.560	21.313	17.143	13.058
Dioguardi and Mele (2015)	19.240	19.040	13.777	14.362	16.465
Wang et al. (2011)	21.374	22.618	27.009	19.958	21.339
Komar and Reimers (1978)	10.406	6.100	25.512	8.980	3.165
Baba and Komar (1981)	11.173	4.268	27.401	11.693	4.863
Komar (1980)	68.173	32.323	25.876	26.451	26.529
Hydrochorous seeds	21.001	31.771	/	/	19.830

Following the idea of Dioguardi et al. (2018), the new model adopts three shaped-modified functions in the spherical drag law of Clift and Gauvin (1971). With these functions based on R_{ep} and ϕ, the new model exhibits better performance than the other models. With the wide range of applicability in both flow regimes and particle shapes, the present model may be practical in solving problems concerning the riverine ecosystem. On the one hand, by relating the settling process of seeds with the dispersal process, more detailed information can be obtained about the germination of seeds and establishment of aquatic vegetation, which is crucial for flow characteristics in river systems (Meier et al. 2013). On the other hand, the advanced settling model can estimate the rate of sediment transport for various particles and flow regimes by being applied in predicting the distribution of sediment concentration (Fu et al. 2005; Graf and Cellino 2002). Such application may be verified when provided with further sediment concentration profile measurements of irregular particles. In addition to its application in the riverine ecosystems, the new settling model may be further improved by extending from the drag of single irregular particle to conglomerates of particles.

Supplementary Information The online version contains supplementary material available at https://doi.org/10.1007/s11356-021-14880-9.

Author contribution All authors contributed to the model conception and derivation. F. Yang: data curation, methodology, formal analysis, writing—original draft; Y.H. Zeng: conceptualization, funding acquisition, supervision, writing—review and editing; W.X. Huai: conceptualization, writing—review and editing. All authors have read and approved the final manuscript.

Funding This work is financially supported by the National Key Research and Development Program of China (No. 2016YFA0600901) and National Natural Science Foundation of China (Nos. 51879197, 51622905).

Availability of data and materials All data generated or analyzed during this study are included in the supplementary information files, which can be found in the online version of this article.

Declarations

Ethical approval and consent to participate Not applicable

Consent for publication Not applicable

Competing interests The authors declare no competing interests.

Notation a, b, c, semi-axes of a tri-axial ellipsoid (m); A_p, projected area perpendicular to the flow direction (m^2); A_s, total surface area of the particle (m^2); A_{sph}, surface area of equivalent spheres (m^2); C_d, drag coefficient (−); $C_{d,\ calc}$, calculated drag coefficient (−); $C_{d,\ meas}$, measured drag coefficient (−); $C_{d,\ sphere}$, drag coefficient of sphere (−); CSF, Corey shape factor (−); d, l, diameters and heights of cylinders and disks (m) (mentioned in Table 2); d_n, diameter of the volume equivalent sphere (m); d_N, nominal particle diameter (m); d_l, d_m, d_s, lengths of the longest, intermediate, and shortest principle axes of the particle (m); D_*, dimensionless particle diameter (−); E, aspect ratio (−); e, elongation (−); f, flatness (−); g, gravitational acceleration ($m\ s^{-2}$); R_{ep}, particle Reynolds number (−); S, the ratio between equivalent sphere area and the projected area of particle settling direction (−); s, h, edge lengths of cubes and cuboids (m) (mentioned in Table 2); V, volume of the particle (m^3); W_s, settling velocity of particles ($m\ s^{-1}$); $W_{s,\ calc}$, calculated settling velocity of particles ($m\ s^{-1}$); $W_{s,\ meas}$, measured settling velocity of particles ($m\ s^{-1}$); X, particle circularity (−); ρ_s, particle density ($kg\ m^{-3}$); ρ_f, fluid density ($kg\ m^{-3}$); μ, dynamic viscosity ($kg\ m^{-1}\ s^{-1}$); υ, kinematic viscosity ($m^2\ s^{-1}$); ϕ, particle sphericity (−); ψ, shape descriptor (−); λ,k, parameters in Eq. (8) (−); α_1, α_2, α_3, exponents in Eq. (14) (a, b, c) (−)

References

Alcerreca J, Silva R, Mendoza E (2013) Simple settling velocity formula for calcareous sand. J Hydraul Res 51:215–219. https://doi.org/10.1080/00221686.2012.753645

Baba J, Komar PD (1981) Settling velocities of irregular grains at low Reynolds numbers. J Sediment Petrol 51:121–128. https://doi.org/10.1306/212F7C25-2B24-11D7-8648000102C1865D

Bagheri G, Bonadonna C (2016) On the drag of freely falling non-spherical particles. Powder Technol 301:526–544. https://doi.org/10.1016/j.powtec.2016.06.015

Bagheri G, Bonadonna C, Manzella I, Vonlanthen P (2015) On the characterization of size and shape of irregular particles. Powder Technol 270:141–153. https://doi.org/10.1016/j.powtec.2014.10.015

Brown PP, Lawler DF (2003) Sphere drag and settling velocity revisited. J Environ Eng 123:222–231. https://doi.org/10.1061/(ASCE)0733-9372(2003)129:3(222

Büttner R, Dellino P, La Volpe L, Lorenz V, Zimanowski B (2002) Thermohydraulic explosions in phreatomagmatic eruptions as evidenced by the comparison between pyroclasts and products from molten fuel coolant interactions experiments. J Geophys Res Solid Earth 107:5–14. https://doi.org/10.1029/2001JB000511

Chambert S, James CS (2009) Sorting of seeds by hydrochory. River Res Appl 25:48–61. https://doi.org/10.1002/rra.1093

Cheng NS (1997) Simplified settling velocity formula for sediment particle. J Hydraul Eng 123:149–152. https://doi.org/10.1061/(ASCE)0733-9429(1997)123:2(149

Cheng NS (2009) Comparison of formulas for drag coefficient and settling velocity of spherical particles. Powder Technol 189:395–398. https://doi.org/10.1016/j.powtec.2008.07.006

Chien SF (1994) Settling velocity of irregularly shaped particles. SPE Drilling and Competition 9:281–289. https://doi.org/10.2118/26121-PA

Clift R, Gauvin WH (1971) Motion of entrained particles in gas streams. Can J Chem Eng 49:439–448. https://doi.org/10.1002/cjce.5450490403

Clift R, Grace JR, Weber ME (2005) Bubbles, drops, and particles. Dover publications, Mineola, New York

Corey AT (1963) Influence of shape on the fall velocity of sand grains. Colorado State University Audio Visual Service

Dellino P, Mele D, Bonasia R, Braia G, La Volpe L, Sulpizio R (2005) The analysis of the influence of pumice shape on its terminal velocity. Geophys Res Lett 32. https://doi.org/10.1029/2005GL023954

Dietrich WE (1982) Settling velocity of natural particles. Water Resour Res 18:1615–1626. https://doi.org/10.1029/WR018i006p01615

Dioguardi F, Mele D (2015) A new shape dependent drag correlation formula for non-spherical rough particles. Experiments and results. Powder Technol 277:222–230. https://doi.org/10.1016/j.powtec.2015.02.062

Dioguardi F, Mele D, Dellino P (2018) A new one-equation model of fluid drag for irregularly shaped particles valid over a wide range of Reynolds number. J Geophys Res Solid Earth 123:144–156. https://doi.org/10.1002/2017JB014926

Fu X, Wang G, Shao X (2005) Vertical dispersion of fine and coarse sediments in turbulent open-channel flows. J Hydraul Eng 131:877–888. https://doi.org/10.1061/(ASCE)0733-9429(2005)131:10(877)

Ganser GH (1993) A rational approach to drag prediction of spherical and non-spherical particles. Powder Technol 77:143–152. https://doi.org/10.1016/0032-5910(93)80051-B

Gogus M, Ipekci ON, Kokpinar MA (2001) Effect of particle shape on fall velocity of angular particles. J Hydraul Eng 127:860–869. https://doi.org/10.1061/(ASCE)0733-9429(2001)127:10(860)

Graf WH, Cellino M (2002) Suspension flows in open channels: experiment study. J Hydraul Res 40:435–447. https://doi.org/10.1080/00221680209499886

Gurnell AM, Thompson K, Goodson J, Moggridge H (2008) Propagule deposition along river margins: linking hydrology and ecology. J Ecol 96:553–565. https://doi.org/10.1111/j.1365-2745.2008.01358.x

Gurnell AM, Bertoldi W, Corenblit D (2012) Changing river channels: the roles of hydrological processes, plants and pioneer fluvial landforms in humid temperature, mixed load, gravel bed rivers. Earth Sci Rev 111:129–141. https://doi.org/10.1016/j.earscirev.2011.11.005

Haider A, Levenspiel O (1989) Drag coefficient and terminal velocity of spherical and non-spherical particles. Powder Technol 58:63–70. https://doi.org/10.1016/0032-5910(89)80008-7

Hallermeier R (1981) Terminal settling velocity of commonly occurring sand grains. Sedimentology 28:859–865. https://doi.org/10.1111/j.1365-3091.1981.tb01948.x

Koch EW, Ailstock MS, Booth DM, Shafer DJ, Magoun AD (2010) The role of currents and waves in the dispersal of submersed angiosperm seeds and seedlings. Restor Ecol 18:584–595. https://doi.org/10.1111/j.1526-100X.2010.00698.x

Komar PD (1980) Settling velocities of circular cylinders at low Reynolds numbers. J Geol 88:327–336. https://doi.org/10.1086/628510

Komar PD, Reimers CE (1978) Grain shape effects on settling rates. J Geol 86:193–209. https://doi.org/10.1086/649674

Lau R, Chuah H (2013) Dynamic shape factor for particles of various shapes in the intermediate settling regime. Adv Powder Technol 24:306–310. https://doi.org/10.1016/j.apt.2012.08.001

Loth E (2008) Drag of non-spherical solid particles of regular and irregular shape. Powder Technol 182:342–353. https://doi.org/10.1016/j.powtec.2007.06.001

Meier CI, Reid BL, Sandoval O (2013) Effects of the invasive plant Lupinus polyphyllus on vertical accretion of fine sediment and nutrient availability in bars of the gravel-bed Paloma river. Limnolog-Ecol Manag Inland Waters 43:381–387. https://doi.org/10.1016/j.limno.2013.05.004

Merritt DM, Wohl EE (2002) Processes governing hydrochory along rivers: hydraulics, hydrology, and dispersal phenology. Ecol Appl 12:1071–1087. https://doi.org/10.1890/1051-0761(2002)012[1071:PGHARH]2.0.CO;2

Ramanujan S (1914) Modular equations and approximations to π. Q J Math 45:350–372

Song XZ, Xu ZM, Li GS, Pang ZY, Zhu ZP (2017) A new model for predicting drag coefficient and settling velocity of spherical and non-spherical particle in Newtonian fluid. Powder Technol 321:242–250. https://doi.org/10.1016/j.powtec.2017.08.017

Swamee P, Ojha C (1991) Drag coefficient and fall velocity of non-spherical particles. J Hydraul Eng 117:660–667. https://doi.org/10.1061/(ASCE)0733-9429(1991)117:5(660)

Taylor MA, Garboczi EJ, Erdogan ST, Fowler DW (2006) Some properties of irregular 3-D particles. Powder Technol 162:1–15. https://doi.org/10.1016/j.powtec.2005.10.013

Terfous A, Hazzab A, Ghenaim A (2013) Predicting the drag coefficient and settling velocity of spherical particles. Powder Technol 239:12–20. https://doi.org/10.1016/j.powtec.2013.01.052

Tran-Cong S, Gay M, Michaelides EE (2004) Drag coefficients of irregularly shaped particles. Powder Technol 139:21–32. https://doi.org/10.1016/j.powtec.2003.10.002

Wadell H (1932) Volume, shape, and roundness of rock particles. J Geol 40:443–451. https://doi.org/10.1086/623964

Wang JS, Qi HY, Zhu JZ (2011) Experimental study of settling and drag on cuboids with square base. Particuology 9:298–305. https://doi.org/10.1016/j.partic.2010.11.002

Wang Y, Zhou LX, Wu Y, Yang Q (2017) New simple correlation formula for the drag coefficient of calcareous sand particles of highly irregular shape. Powder Technol 326:379–392. https://doi.org/10.1016/j.powtec.2017.12.004

White, F. M. (1998). Fluid mechanics. Mcgraw-Hill College.

Yoshikawa M, Hoshino Y, Iwata N (2013) Role of seed settleability and settling velocity in water for plant colonization of river gravel bars. J Veg Sci 24:712–723. https://doi.org/10.1111/jvs.12001

Zhu X, Zeng YH, Huai WX (2017) Settling velocity of non-spherical hydrochorous seeds. Adv Water Resour 103:99–107. https://doi.org/10.1016/j.advwatres.2017.03.001